USGS
science for a changing world

# Candidate-Penetrative-Fracture Mapping of the Grand Canyon Area, Arizona, from Spatial Correlation of Deep Geophysical Features and Surficial Lineaments

Digital Series 121

U.S. Department of the Interior
U.S. Geological Survey

# Candidate-Penetrative-Fracture Mapping of the Grand Canyon Area, Arizona, from Spatial Correlation of Deep Geophysical Features and Surficial Lineaments

By Mark E. Gettings and Mark W. Bultman

Digital Series 121

**U.S. Department of the Interior**
**U.S. Geological Survey**

**U.S. Department of the Interior**
Gale A. Norton, Secretary

**U.S. Geological Survey**
Charles G. Groat, Director

U.S. Geological Survey, Reston, Virginia: 2005

For sale by U.S. Geological Survey Information Services
Box 25286, Denver Federal Center
Denver, CO 80225

This report and any updates to it are available online at:
http://pubs.usgs.gov/ds/121/

For additional information write to:
U.S. Geological Survey
Box 25046, Mail Stop 421, Denver Federal Center
Denver, CO 80225-0046

Additional USGS publications can be found at:
http://geology.usgs.gov/products.html

For more information about the USGS and its products:
Telephone: 1–888–ASK–USGS (1-888-275-8747)
World Wide Web: http://www.usgs.gov/

Any use of trade, product, or firm names in this publication is for descriptive purposes only and does not imply endorsement by the U.S. Government.

Although this report is in the public domain, it may contain copyrighted materials that are noted in the text. Permission to reproduce those items must be secured from the individual copyright owners.

**Cataloging-in-Publication data are on file with the Library of Congress (URL http://www.loc.gov/).**

Produced in the Western Region, Menlo Park, California
Manuscript approved for publication, April 20, 2005
Text edited by George A. Havach
Layout and design by Stephen L. Scott

# Contents



## Figures

## Tables

# Candidate-Penetrative-Fracture Mapping of the Grand Canyon Area, Arizona, from Spatial Correlation of Deep Geophysical Features and Surficial Lineaments

By Mark E. Gettings and Mark W. Bultman

## Abstract

Some aquifers of the southwestern Colorado Plateaus Province are deeply buried and overlain by several impermeable shale layers, and so recharge to the aquifer probably is mainly by seepage down penetrative-fracture systems. The purpose of this 2-year study, sponsored by the U.S. National Park Service, was to map candidate deep penetrative fractures over a 120,000-km$^2$ area, using gravity and aeromagnetic-anomaly data together with surficial-fracture data. The study area was on the Colorado Plateau south of the Grand Canyon and west of Black Mesa; mapping was carried out at a scale of 1:250,000. The resulting database constitutes a spatially registered estimate of deep-fracture locations. Candidate penetrative fractures were located by spatial correlation of horizontal-gradient and analytic-signal maximums of gravity and magnetic anomalies with major surficial lineaments obtained from geologic, topographic, side-looking-airborne-radar, and satellite imagery. The maps define a subset of candidate penetrative fractures because of limitations in the data coverage and the analytical technique. In particular, the data and analytical technique used cannot predict whether the fractures are open or closed. Correlations were carried out by using image-processing software, such that every pixel on the resulting images was coded to uniquely identify which datasets are correlated. The technique correctly identified known and many new deep fracture systems. The resulting penetrative-fracture-distribution maps constitute an objectively obtained, repeatable dataset and a benchmark from which additional studies can begin. The maps also define in detail the tectonic fabrics of the southwestern Colorado Plateaus Province. Overlaying the correlated lineaments on the normalized-density-of-vegetation-index image reveals that many of these lineaments correlate with the boundaries of vegetation zones in drainages and canyons and so may be controlling near-surface water availability in some places. Many derivative products can be produced from the database, such as fracture-density-estimate maps, and maps with the number of correlations color-coded to estimate the possible quality of correlation. The database contained in this report is designed to be used in a geographic information system and image-processing systems, and most data layers are in georeferenced tagged image format (Geotiff) or ARC grids. The report includes 163 map plates and various metadata, supporting, and statistical diagram files.

## Introduction

The Colorado Plateau south of the Colorado River and west of the Little Colorado River is the source area for ground-water recharge to the deep aquifers feeding the springs and seeps on the south side of Grand Canyon National Park (Robson and Banta, 1995). The U.S. National Park Service sponsors research on the hydrologic system of the area to assist in managing the park. This part of the plateau is sparsely populated and relatively undeveloped; it has few deep boreholes, and so little is known of its geology and hydrology except at regional scales. Because several of the aquifers are beneath basically impermeable shale formations, most recharge is believed to be by way of penetrative fractures rather than percolation (Robson and Banta, 1995). Thus, knowledge of the deep-penetrative-fracture distribution may be helpful in managing ground-water resources. This report provides a set of maps of candidate deep fractures the southwestern Colorado Plateaus Province, located by vertical spatial correlation of surficial fractures with the lineaments of deep structure derived from an analysis of gravity and aeromagnetic data.

The study area (fig. 1) comprises six 1:250,000-scale quadrangles covering the southwestern part of the Colorado Plateau in Arizona. Although this area includes some parts of the plateau north of the Colorado River and parts of the Transition Zone and Basin and Range Provinces, it was easier and more appropriate from a structural-geologic standpoint to include the entire quadrangles rather than mask out parts not on the plateau. An area of one 1:250,000-scale sheet, approximately centered on Grand Canyon Village on the south rim of the Grand Canyon, was designated the focus area (fig. 1), made up of four quarters of the surrounding quadrangles. Within the focus area, a map was hand drawn from the standard correlation images produced for all quadrangles. Although the map does not contain as much information as the correlation images, it is useful for overlaying onto other maps and for delineating subtle throughgoing trends not obvious on other images.

## Method

In many areas characterized by thick surficial layers of sedimentary rocks, mapping of deep penetrative fractures has become an important undertaking (see Robson and Banta,

1995, for examples in the United States). Flat-lying sedimentary sequences commonly compose significant parts of basins and plateaus, and if they contain regional aquitards, such as shale, mudstone, siltstone, or some limestone formations, the vertical hydraulic conductivity is essentially zero except where the sequence is broken by steeply dipping fractures. In these environments, except where the aquifer is structurally brought to the surface, the only significant recharge to deep aquifers is by way of deep penetrative fractures (de Marsily, 1986; Ingebritsen and Sanford, 1998), and so mapping probable fractures is an important objective for ground-water studies.

Price (1966, 1974; see Hancock, 1969, and Jaeger and Cook, 1976) showed that penetrative joint and fault systems will form in large sedimentary basins owing to the stresses

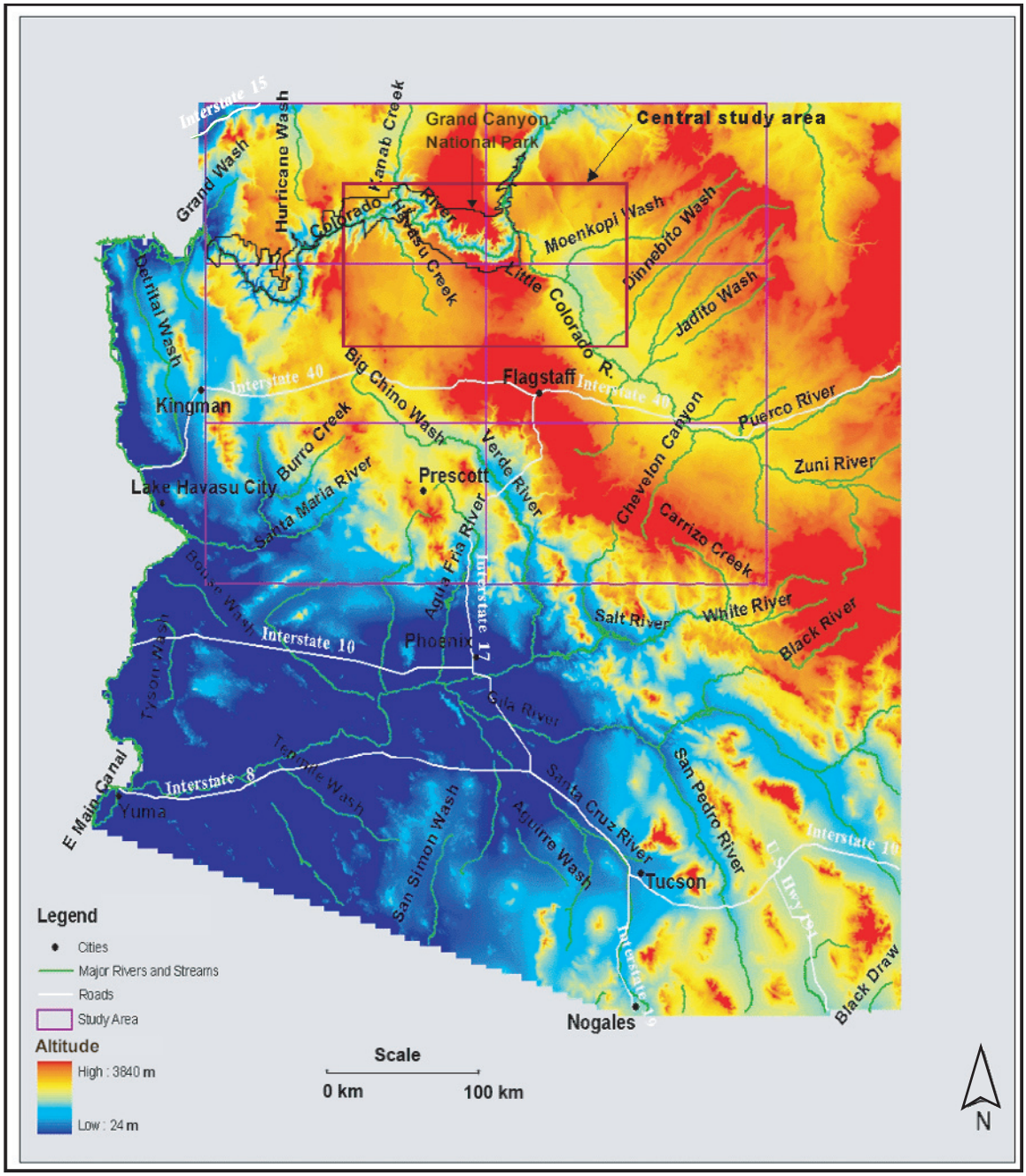


**Figure 1.** Arizona, showing location of study area comprising six 1:250,000-scale quadrangles, from top to bottom: Grand Canyon, Williams, and Prescott in the west (left) and Marble Canyon, Flagstaff, and Holbrook in the east (right). Focus area (heavy-outlined rectangle) includes a quarter each of the Grand Canyon, Marble Canyon, Williams, and Flagstaff quadrangles. The Black Mesa area is high upland of Moenkopi, Dinnebito, and Jadito Washes.

involved during downwarp, lithification, and subsequent uplift, even without deformation due to external stresses. Existing stress fields due to tectonic forces will superpose on the basinal stresses and modify the overall stress field and consequent fracture pattern. Thus, most fracturing from jointing as well as faulting will generally be penetrative throughout the entire sedimentary section as it existed at the time of fracture formation. Whether or not the fractures remain open or are closed depends on the rheology of the rocks, the chemistry of interstitial and circulating fluids, and the regional tectonic history. For example, a sedimentary section in an extensional-stress regime will more likely have a higher proportion of open fractures than one in a compressional-stress regime, and some geochemical ground-water regimes can result in precipitation of fracture-sealing minerals. Odling and others (1999) provided an excellent review of fracture systems in sedimentary sections and their resulting permeabilities for fluid flow in fractures. The present study does not address the question of openness of fractures other than to note that the overall stress regime in the study area (fig. 1) has been extensional for much of Tertiary and Quaternary time (Huntoon, 1990).

Here, we assume that the geologic environment is a thick (1–3 km) section of sedimentary rocks overlying heterogeneous crystalline basement rocks with contrasting magnetization and density. We assume the sedimentary rocks to be flat-lying or only gently deformed, with a uniform magnetization and density for each layer, and that bedding-plane hydraulic conductivity is not a factor, other than possibly providing horizontal conduits to fracture systems where the water can seep to deep levels. Our strategy was to map structures in the basement that are likely to generate fractures, mainly fault and fold axes, and to superimpose this map on a surficial-fracture map derived from geologic and other shallow data. Coincidences of candidate deep fractures down dip from surface fractures define likely penetrative fractures. Maps of likely deep-fracture, fault, and fold axes were prepared by interpretation of curvilinearly persistent features on gravity- and magnetic-anomaly maps. A primary tool for this interpretation is the location of local horizontal-gradient maximums, as described by Blakely and Simpson (1986) and Grauch and Cordell (1987). These workers showed that for relatively steeply dipping to vertical contacts between rocks with differing magnetic and (or) density properties, the maximum horizontal gradient in the gravity or pseudogravity transformation of the magnetic-anomaly field will be nearly vertical over the contact between the two differing rock types.

These assumptions are validated by direct observation in the Grand Canyon area (fig.1), where surficial faults and fractures on the sedimentary plateau are directly traceable down the canyon wall into structures in the underlying metamorphic and igneous rocks of the basement (figs. 2, 3). The Bright Angel Fault zone (Huntoon, 1990), for example, offsets both sedimentary and basement rocks. Most side canyons and changes in river-course direction in the study area are related to differential weathering along penetrative fractures. Crystalline basement rocks in the Bright Angel Canyon area (fig. 3) consist of highly deformed amphibolitic schist with numerous injections of granitic rocks. The schist is relatively magnetic and dense in comparison with the granitic rocks. In addition to the faults and fractures, the lithologic contacts are steeply dipping to vertical and have strong physical-property differences, and so the basement is ideal for producing contrasting signatures in the geophysical data. The basement in much of the Grand Canyon area was an erosional surface before the beginning of sedimentation during the Precambrian (Babcock, 1990), and so differential erosion due to different rock types has associated topographic differences with density and magnetization contrasts, in addition to contrasts due to offsets on fractures and faults. Subsequent folding events (Beus and Morales, 1990) probably caused or enhanced fracturing in the sedimentary section along the fold axes and may have created geophysical lineaments by uplift/subsidence in the basement rocks owing to the folding. The geologic history of the Colorado Plateaus Province documents more than 20 separate regional tectonic events of either uplift or subsidence in the study area in the past 1.7 b.y., including some activity during the Holocene (Beus and Morales, 1990). Therefore, we assume that virtually all fractures and faults within the basement have moved up and down multiple times, with consequent fracturing effects on the overlying sedimentary strata. Most probably, at least some of these events resulted in new fractures and faults penetrating both the basement and overlying sedimentary rocks.

Modeling may be required to resolve ambiguities in the locations of gradient maximums with respect to the actual fault, fracture, or fold axis. In this study, we used analytic-signal maximums (Nabighian, 1972) as an additional structural indicator and a means of defining the dip of deep structures. If the deep structure has dipping boundaries, the horizontal-gradient maximums will be displaced downdip from the analytic-signal maximums, thus allowing the dip to be estimated. If magnetic horizons (for example, volcanic flows) are present within the sedimentary section and if evidence exists of significant nonvertical dip of fracture systems, an intermediate-depth layer must be included in the model. No such horizons were required in this study.

Maps of surficial fractures were prepared by using geologic maps, aerial photographs, satellite images, topographic maps, and any other remote-sensing data available. The deep- and surficial-fracture maps were then superimposed, and candidate penetrative fractures were defined from an analysis of coincident or nearly coincident features. If the surficial fractures dip significantly, this fact must be taken into account by using depth estimates computed from the gravity- and magnetic-anomaly data. In this study, we used regional gravity- and aeromagnetic-anomaly data defined on a 500-m grid, and so the data have been low-pass filtered by the grid-generation process. To account for the uncertainty in gradient locations due to the gridding process, we allowed correlations within ±1/2 grid unit of a deep gradient, automatically allowing for dips of about ±40º between the deep structure and the surface for a typical depth to basement of about 1 km, which is representative for the study area (fig. 1).

**Figure 2.** Grand Canyon of the Colorado River (fig. 1), showing nearly horizontally stratified sedimentary rocks of the Colorado Plateau overlying metamorphic and igneous basement rocks. Note vertical continuity of erosional breaks and side drainages from top of plateau into basement, suggesting that erosion follows penetrative fractures. View northward from South Kaibab Trail.

This method has several sources of difficulty. For the deep-fracture pattern, a lack of sufficiently precise or closely spaced gravity- and aeromagnetic-anomaly data will mean that not all anomalies are detectable, and so lineaments, especially subtle ones, will be lost. If fracture or fault systems do not juxtapose rocks with contrasting density or magnetization, no anomaly will be detected, or a lithologic contact with no relative motion may coincide with a shallow lineament with no intervening penetrative fracture, thus giving a false correlation. For the shallow-fracture dataset, lack of sufficiently precise data is a limitation, and some anthropogenic factors may lead to false identifications. Our experience suggests that at the scale used in this study (1:250,000), anthropogenic lineaments are quite rare. Powerlines, fences, roads, and freeways do not show up clearly in the correlations, if at all, because of their negligible associated geophysical anomalies. The one anthropogenic correlation we have observed is railway tracks, which are easily visible in satellite imagery and have a significant associated magnetic anomaly. Shallow burial by surficial deposits may obscure fractures. We believe that the net result of these sources of error, in mathematical terms, is that the set of candidate penetrative fractures defined by this method is a (not the least) lower bound on the total set of actual penetrative fractures.

The three derived deep-structural-trend sets—aeromagnetic anomaly, Bouguer gravity anomaly, and isostatic-gravity anomaly—were correlated vertically with the surficial-trend

**Figure 3.** West wall of The Box in Bright Angel Canyon in Grand Canyon National Park, Ariz. (fig. 1), showing metamorphic and igneous basement rocks. Pink zones are granitic rocks, and gray-green zones are amphibolitic schist.

sets by using an image-processing system. The data sources and data-processing methods are described in the next sections. This method produced a red-green-blue (RGB) image of correlations, with Bouguer gravity anomaly in the red channel, isostatic-gravity anomaly in the green channel, and aeromagnetic anomaly in the blue channel. In the resulting images, uncorrelated pixels in each of the three channels were set to 0 (black), and pixels that correlated with surficial datasets were assigned nonzero numbers coded to show with which of the surficial datasets the deep data were correlated (fig. 4). In each channel, a correlation with geology was set to 1, with topography to 2, with the thematic mapper to 4, and with side-looking airborne radar (SLAR) to 8. Using this scheme, the sum of the numbers is unique for every combination of correlations, so that no information is lost. Thus, each channel is assigned a number between 0 and 15 for every pixel covering the study area (fig. 1). For example, values of 7 in the red channel and 0 in the green and blue channels indicates that a Bouguer gravity anomaly correlates with geology, topography, and thematic mapper, and that isostatic-gravity and aeromagnetic anomalies do not correlate with any surficial features. The numerical values assigned to pixels in the red (Bouguer gravity), green (isostatic gravity), and blue (aeromagnetic anomaly) channels are listed below.

| *Numerical value* | *Surficial datasets that correlate with the deep dataset* |
|---|---|
| 0 | No correlation. |
| 1 | Geology. |
| 2 | Topography. |
| 3 | Geology + Topography |
| 4 | Thematic mapper. |
| 5 | Thematic mapper+geology. |
| 6 | Thematic Mapper + Topography |
| 7 | Thematic mapper+geology+topography. |
| 8 | SLAR. |
| 9 | SLAR+geology. |
| 10 | SLAR+topography. |
| 11 | SLAR+geology+topography. |
| 12 | SLAR+thematic mapper. |
| 13 | SLAR+thematic mapper+geology. |
| 14 | SLAR+thematic mapper+topography. |
| 15 | SLAR+thematic mapper+geology+topography. |

# Data Compilation and Sources

## Geophysical Data

Existing aeromagnetic-anomaly, Bouguer gravity-anomaly, and isostatic gravity-anomaly data for Arizona (Sweeney and Hill, 2001) were used in this study in the form of regular grids with a value at 500-m intervals. The grid interval constitutes a low-pass filter on the data so that the precise locations of such anomaly features as gradient maximums, even though interpolated from the grid values, are indeterminable at distances less than about half a grid interval. This fact determined that the scale of the correlation analysis would be 1:250,000, so that a grid interval of 500 m spans 2 mm at the map scale. Moreover, in some parts of the study area (fig. 1), the density of observed gravity and (or) aeromagnetic data is too sparse to justify interpretation at larger scales, for example, 1:100,000. If the images obtained from this study are used at larger scales, this uncertainty in the location of deep structural features must be borne in mind.

## Surficial Data

Four types of Earth surface data were used to detect curvilinear features (lineaments) expressed at the Earth's surface: (1) U.S. Geological Survey (USGS) SLAR, (2) Landsat 7 thematic-mapper (TM) panchromatic imagery, (3) USGS digital elevation models (DEMs), and (4) USGS geologic mapping.

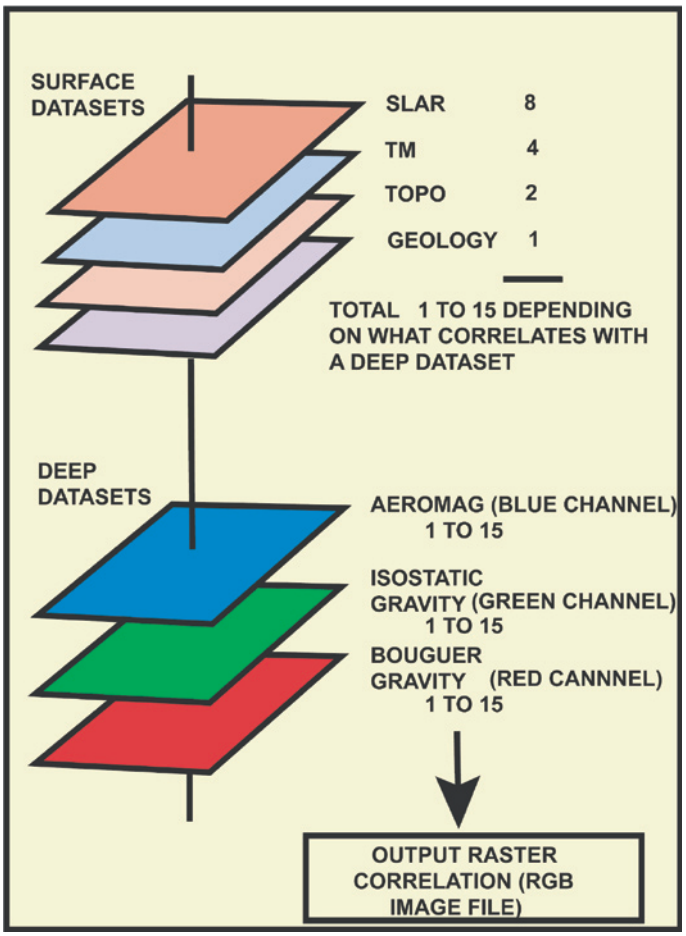


**Figure 4.** Schematic diagram of scheme used to uniquely define correlations between surficial and deep datasets. Pixel values in output image range from 0 to 15 in each of three (red, blue, and green) channels.

Digital-orthophoto-quarter-quadrangle (DOQQ) aerial photography was considered to provide detail beyond the scope of this study.

## Geophysical Data Processing

The three geophysical datasets were first divided into subgrids covering each of the six 1:250,000-scale quadrangles of the study area (fig. 1). Each grid extended several rows and columns beyond its respective quadrangle boundary to reduce discontinuities in the trend analysis at neighboring quadrangles. For each quadrangle, the aeromagnetic data were transformed from dipolar to a form in which the dipolar maximums and minimums have coincident axes, using the "reduction to pole" transformation (for example, Blakely, 1995). This transformation is needed to prevent distortion of the structural trends mapped by the aeromagnetic anomaly at points other than the magnetic poles, owing to the dipolar form of magnetic anomalies. For completeness and to enable evaluation of the possible effects of remnant magnetization, shaded-relief images of the aeromagnetic anomaly (not reduced to pole), Bouguer gravity anomaly, and isostatic-gravity anomaly were prepared, illuminated from the northeast and northwest, respectively, for a total of six maps. These maps allow checking of the validity of the trendlines generated on the computer, as described below. Additionally, the maps are valuable in the study of the various areas as an overlay to geologic and geographic data. For each of the three grids (aeromagnetic anomaly reduced to pole, Bouguer gravity anomaly, and isostatic-gravity anomaly), the maximums of horizontal gradient and analytic signal were calculated and stored as a set of ($x$, $y$) points locating the maximums on the map. All map manipulation and analysis was done with the Oasis Montaj software produced by Geosoft, Inc., of Toronto, Ontario, Canada, supplemented with several GX plug-ins produced by the USGS (J. Phillips, written commun., 2003). A typical shaded-relief map with the derived trendlines (lineaments) superposed is shown in figure 5.

Although the use of Bouguer gravity anomaly and isostatic-gravity anomaly may seem redundant, we found significant trends in each dataset absent in the other. In general, the isostatic-gravity anomaly is just the Bouguer gravity anomaly corrected for topography on the basis of some crust-mantle-compensation model, and so the isostatic-gravity anomaly should represent more shallow crustal sources. We have no guarantee, however, that at least some sources of the Bouguer gravity anomaly are not shallower, with a large horizontal

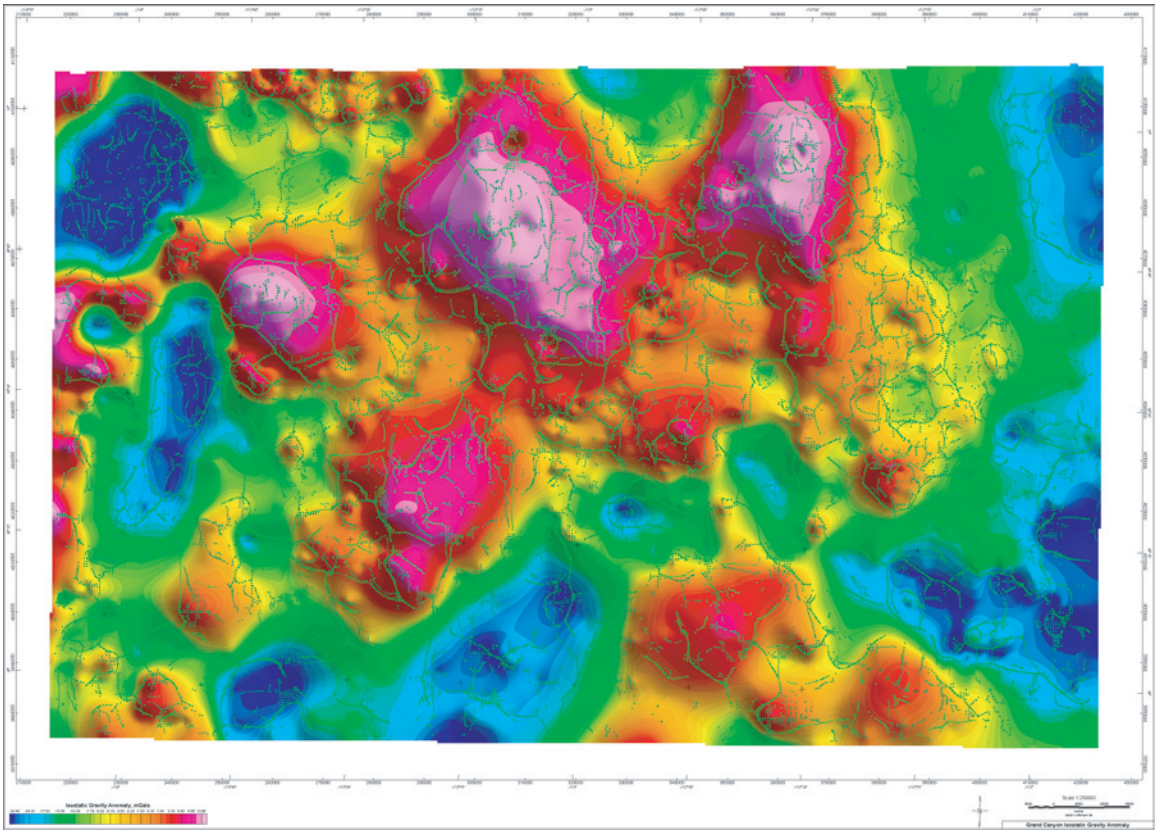

**Figure 5.** Typical shaded-relief map of geophysical data (here, isostatic-gravity-anomaly map of the Grand Canyon quadrangle; see fig. 1), with superimposed maximums for horizontal gradient (light green) and analytic signal (dark green). Illumination is from northeast (upper right).

extent, such as a facies change, and so shallow crustal events may be affected by deeper structures. For this reason, we used both the Bouguer gravity- and isostatic-gravity-anomaly fields to define trends.

A trend analysis was performed on the horizontal-gradient grid of each of the three anomaly grids for all six quadrangles. Although every anomaly has trends going around it in a complete circuit, any elongation or preferred orientation will show up as a peak above the uniform background in the distribution of trends if a uniform spatial sample is observed. The grid has a uniform spatial sample, and so a histogram or rose diagram of the strike of the horizontal gradient at each gridpoint provides an unbiased sample of all trends. Peaks in this distribution represent the trend directions of noncircular anomalies and map the directions of boundaries between various magnetic and density contrasts (Gettings, 2001). This procedure was carried out for the horizontal gradient of the reduced-to-pole-aeromagnetic-anomaly, Bouguer gravity-anomaly, and isostatic-gravity-anomaly grids. At each gridpoint, the perpendicular to (strike direction of) the gradient was computed and recorded on a histogram and rose diagram.

The rose diagrams for the strikes of the three anomalies for each of the six quadrangles are summarized in figure 6. These diagrams vary significantly from quadrangle to quadrangle, indicating variations in tectonic regime.

Bouguer gravity anomalies in the Prescott quadrangle in the southwest (fig. 1) show a strong peak in the northwestward direction corresponding to the large-scale northwest-trending structures in the Transition Zone from the Colorado Plateaus Province to the Basin and Range Province. In this quadrangle, the aeromagnetic- and, to a lesser extent, isostatic-gravity-anomaly trends are strongly north to northeast, corresponding to the smaller structures and rock types in the Prescott area with a strong northward to northeastward trend. The Williams and Grand Canyon quadrangles show dominantly north-southward and northeastward trends, as well as lesser northwestward and east-westward trends. The eastern column of quadrangles shows dominantly northeastward trends but with large differences between the Marble Canyon quadrangle and the two quadrangles to the south. The Marble Canyon quadrangle also has strong sets of lineaments trending north-south, northwest, and east-west. We note that although most of the maps show strong northeast and northwest lineaments (see fig. 5), all the quadrangles contain subsets of approximately north-south and east-west lineaments. The 18 rose diagrams (and their corresponding histograms) contain much information related to the tectonic history of the southwestern Colorado Plateaus Province that deserves further study.

The datasets used in the analysis described here would also be useful for further study, and so they are included on the accompanying DVD disc as a convenience for future researchers. A total of 21 products for each quadrangle are derived from the aeromagnetic- and gravity-anomaly data:

1. Complete Bouguer gravity-anomaly, isostatic-gravity-anomaly, and aeromagnetic-anomaly shaded-relief images illuminated from northeast and southeast. The northeast-illuminated images include symbol plots of the locations of all horizontal-gradient-magnitude maximums (light color) and analytic-signal maximums (dark color), for a total of six georeferenced-tagged-image-format- (Geotif) maps per quadrangle (universal-transverse-mercator [UTM] projection, NAD27 datum).
2. ARC/INFO shapefiles of the symbols, locating horizon tal-gradient magnitudes and analytic signals for complete Bouguer gravity-anomaly, isostatic-gravity-anomaly, and aeromagnetic-anomaly (UTM projection, NAD27 datum) grids, for a total of six shapefiles.
3. Complete Bouguer gravity-anomaly, isostatic-gravity-anomaly, and aeromagnetic-anomaly (UTM projection, NAD27 datum) grids, in Geosoft grid-exchange format, for a total of three ASCII text files.
4. Histograms and rose diagrams of the strike of the horizontal gradient for all gridpoints on each of the three grids (complete Bouguer gravity, isostatic gravity, and aeromagnetic anomalies), for a total of six tagged-image-format (TIF) images.

## Surficial Data Processing

Several lineament-extraction methods were evaluated for each type of surface-feature data. The method chosen in each case (see discussion below) was based on a subjective visual determination of which produced the best set of lineaments for each type of data. Lineaments were extracted from the data at the original resolution of the data. All surficial-lineament products were interpolated to 30-m pixel size for correlation with the geophysical data. Data processing of the surficial-imagery datasets was done with the image-processing software system ENVI produced by Research Systems, Inc. Several programs were written in this system by the second author, using Interactive Display Language (IDL) to accomplish the correlations, create the threshold images, and produce the pixel-encoded RGB correlation images.

Two general problems appeared in the extraction of curvilinear surface features (surface lineaments) from the data. First, because the lineament-extraction method must be sensitive enough to identify surface lineaments in both flat and rugged topography, the spatial density of lineaments extracted from the data is much higher in areas with large topographic relief. Second, linear cultural features were extracted from both the SLAR and TM imagery. No known cultural lineaments were correlatable with geophysical lineaments over distances long enough that they might be confused with a significant hydrologic structure except for railway tracks, which have a significant associated aeromagnetic anomaly; however, railways are sparse in the study area (fig. 1), their route is well known, and so they are easily accounted for.

The surficial datasets used for curvilinear-surface-feature extraction and the lineament-extraction methods used are discussed below.

## Side-Looking-Airborne-Radar Dataset

In the SLAR technique, radar energy is transmitted perpendicular to the aircraft's flightpath. The returned signal is a function of the reflectivity and geometry of the objects reflecting the radar energy back to the aircraft. This signal is processed to produce an amplitude/time video signal, with brighter pixels indicating higher energy returns, creating a series of image strips that are combined into an image of an area. The SLAR images are optically digitized at a pixel size of about 25 m. Because SLAR illuminates the terrain at an oblique angle, it enhances topographic and geologic features and so is ideally suited to the detection of geologically based curvilinear features (Littlesand and Kiefer, 1994; European Space Agency, 2004).

Lineaments were extracted from the SLAR data in this analysis on the basis of the calculated interpixel variance within a moving window. A three- by three-pixel moving window was applied to the data, and the variance of the nine pixel values in the window was calculated and assigned to the

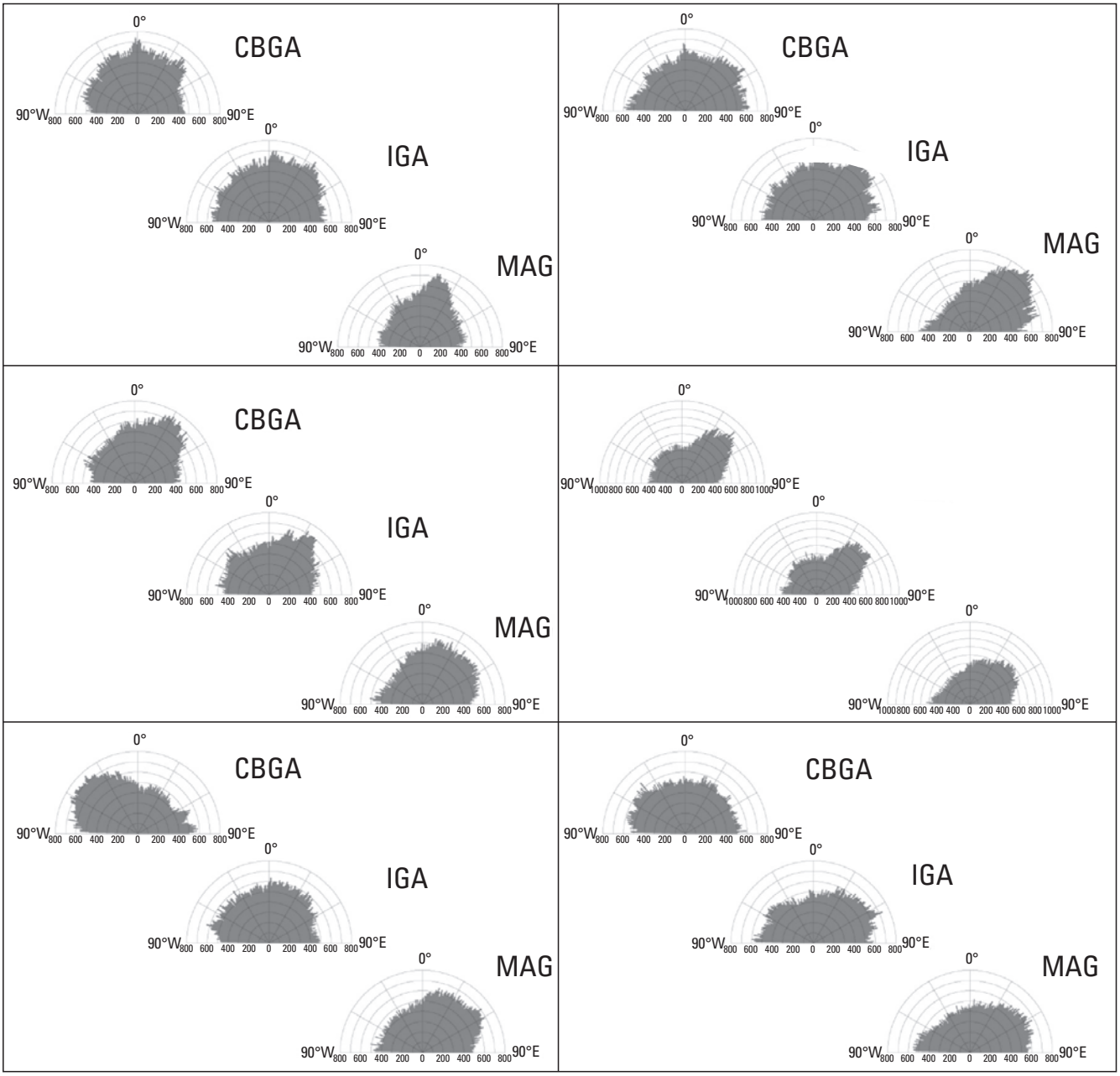


**Figure 6.** Composite rose diagrams for strike of horizontal gradient of complete Bouguer gravity anomaly (CBGA), isostatic gravity anomaly (IGA), and aeromagnetic anomaly (MAG) for each of six 1:250,000-scale quadrangles in study area (fig. 1), from top to bottom: Grand Canyon, Williams, and Prescott in the west (left) and Marble Canyon, Flagstaff, and Holbrook in the east (right). Note changes in distribution of trends for each quadrangle.

location of the window's center pixel. The image of all center pixels produces a new image that maps textures and highlights lineaments (areas where pixel values in the original image change rapidly). The variance value of these images ranges from near 0 to more than 100,000, with a mean of 300 to 500, dependent on the type of terrain that the image encompasses. To highlight the important curvilinear features obtained, all variances smaller than a selected chosen minimum (threshold value) were eliminated. In this analysis, the minimum variance was chosen subjectively but was close to the mean. The minimum variances used to truncate each variance image for the six 1º by 2º quadrangles are as follows:

| *Quadrangle* | *Minimum variance (relative units squared)* |
|---|---|
| Flagstaff | 300 |
| Grand Canyon | 300 |
| Holbrook | 500 |
| Marble Canyon | 400 |
| Prescott | 300 |
| Williams | 300 |

The final lineament image took all variances above the threshold value and set them equal to 1 to produce a binary lineament map.

## Thematic Mapper Dataset

TM multispectral imagery obtained from the Landsat 7 satellite was also used for the detection of curvilinear features on the Earth's surface. This satellite has the latest version of the multispectral scanner (called the Enhanced Thematic Mapper Plus, here referred to as TM), which is capable of obtaining panchromatic images with a spatial resolution of 15 m per pixel. This panchromatic image (TM band 8) provides an increased ability to resolve and detect curvilinear features on the Earth's surface relative to previous Landsat satellites.

The TM data used in this study were acquired in early October 1999. These data provide good lineament detection in the panchromatic band, as well as producing images designed to detect vegetation (Kidwell, 1990), which are referred to as normalized-density-of-vegetation-index (NDVI) images. NDVI images are generally computed by using an infrared (IR) and a visible (VI) band from the satellite data. NDVI is then the quotient of the difference in the two images over the sum: (IR–VI)/(IR+VI). The NDVI images were used to test whether correlations between mapped curvilinear linear geophysical anomalies and surface lineaments are related to the occurrence of vegetation where the lineaments intersect canyons.

Lineaments were extracted from the TM data by using convolution with a directional kernel. This method convolves a three- by three- pixel kernel with the TM image in question. The kernel used in the convolution enhances features along a specific direction. For this study, four principal azimuths were used: 000°, 045°, 090°, and 135°. Because each convolution results in a separate image, with most lineaments running in the direction of the specific kernel direction, the four images were summed to produce a final lineament image. The convolution yields a large range of values, and so a high-pass filter was applied to the image to select only persistent features. The minimum sums (cutoff values) of the convolution products for each quadrangle, omitting below the minimum, are as follows:

| *Quadrangle* | *Minimum sum of convolution products (relative units)* |
|---|---|
| Flagstaff | 150 |
| Grand Canyon | 150 |
| Holbrook | 150 |
| Marble Canyon | 150 |
| Prescott | 200 |
| Williams | 150 |

All values at or above the minimum for each quadrangle were set to 1 to produce a binary lineament map.

## Digital-Elevation-Model Dataset

DEM data were also used to detect curvilinear features in the Earth's surface. These data numerically represent the topography of the Earth's surface and so include information on the direct or indirect response of the Earth's surface to geology. The DEM data used here are from the National Elevation Dataset (NED), which has a 30-m spatial resolution, the highest available over the entire study area (fig. 1).

The method chosen for lineament extraction from the DEM data uses the locations of local horizontal-gradient maximums (Blakely and Simpson, 1986), the same method used to detect geophysical anomalies. Here, this method was applied to topographic data, and it did an excellent job of obtaining curvilinear features from the data, evidently because of a relation between the topography and curvilinear geologic features, mainly faults and fractures, resulting in topographic relief along fractures and faults.

## Geologic-Mapping Dataset

The geologic component of the surface-lineament data relies solely on the mapping of faults and folds within the study area (fig. 1) at scales of 1:1,000,000 (Arizona Geologic Survey and Bureau of Land Management, 1993), 1:500,000

(Hirschberg and Pitts, 2000), and 1:100,000 (in the Grand Canyon 1:100,000-scale quadrangle only; Billingsley, 2000).

## Examples of Lineaments Obtained in the Analysis

Examples of surface-feature lineaments extracted from the four datasets discussed above are shown in figure 7. The finer texture apparent on the TM band 8 image is due to the 15-m spatial resolution of the TM data, almost double the 25-m resolution of the SLAR data and exactly double the 30-m resolution of the DEM data. The parallel lineaments (faults or folds) visible in the geologic-mapping image are due to mapping at different scales and the positioning errors associated with those scales.

The major northeast-trending fault or fold visible in the west-central part of the geologic-mapping image is especially apparent in the DEM images, less apparent in the TM images, and barely visible in the SLAR images. Topographic features of the Grand Canyon are visible in the northeast corner of the SLAR, TM, and DEM images. In addition, lineaments appear in each image that are not observed in any of the others. We assume that this lineament derived from four different types of data will encompass most of the geologically related surface lineaments in the study area (fig. 1).

# Results

The data archive on the accompanying DVD disc contains the various datasets and their supporting metadata, as discussed above. Most data layers are in Geotiff geographically registered format or in files appropriate for import into an ARC/INFO GIS. In particular, the ARC grids for each of the six quadrangles and the focus area (fig. 1) give the final correlations numerically coded from 0 to 15 for each 30-m pixel, as discussed above. These grids which are called correlation maps, constitute the final products of this analysis and map the locations of candidate deep penetrative fractures in the study area. As described above, the archive also contains all supporting data used in the analysis and several visualizations and summaries of the correlations, for a total of 163 map plates, in addition to the various metadata, supporting files, and statistical diagrams.

Below is a description of the various types of map that correlate the geophysical and surface features for each quadrangle in the study area and the focus area (fig. 1). The maps are all available in the "Report Downloads" or the "Project Products and Database" sections of the archive. For each product maps, data are valid only within the actual 1° by 2° quadrangle portrayed on that map. Although data outside the 1° by 2° quadrangle may be shown, the product of the analysis may be invalid in this area because different data used in the analysis may have had a different geographic extent.

## Correlation Maps

The correlation maps, numbered 0 through 15 as described above, are presented as ARC/INFO coverage in which each map is an ARC/INFO grid. The coverage includes a correlation product for each of the three geophysical datasets, as well as an RGB product in which the complete Bouguer gravity-anomaly correlations are shown in red, the isostatic-gravity-anomaly correlations in green, and the aeromagnetic-anomaly correlations in blue. Within each color, pixel values can be accessed, and the exact surface-feature correlation can be obtained as described above (see table 1). These maps, as well as the other product maps, are named for their location: for example, in the focus area ("fa"), correlation maps are named "fa_correlations". Similarly, the Grand Canyon ("gc") 1º by 2º quadrangle correlation maps are named "gc_correlations". The other map names follow that pattern by using an abbreviation for the map area to prefix the map content.

## Correlation Normalized-Density-of-Vegetation-Index Map

The Correlation NVDI maps are Geotiff images with an overlay of all correlations. The correlations are not keyed to either geophysical data or surface-lineament data but are all presented in one color to make the map as readable as possible. Brighter pixels in the NDVI image show areas with more active chlorophyll vegetation. In the focus area (fig. 1), this map is named "fa_ndvi_cor".

## Correlation Digital-Raster-Graphics Map

The correlation digital-raster-graphics (DRG) maps present the geophysical surface-lineament correlations overlain on geographic DRG maps, providing a geographic reference for the correlations. A special coding is used for the correlations on this map. Because the 0 -15 numerical codes would obscure geographic features, these correlations were coded only to specific geophysical data on the DRG map. Where surface-lineament (SL) data are correlated only with complete Bouguer anomaly (CBA) data, the correlations are shown in red; where SL data are correlated only to isostatic-gravity-anomaly (IGA) data, the correlations are shown in green; and where SL data are correlated only to aeromagnetic-anomaly (MAG) data, the correlations are shown in blue. The following combinations of correlations are also shown: SL data correlated to CBA and IGA data are shown in yellow, SL data correlated to CBA and MAG data are shown in magenta, SL data correlated to IGA and MAG data are shown in cyan, and SL data correlated to CBA, IGA, and MAG data are shown in black. In the focus area (fig. 1), this map is named "fa_drg_cor".

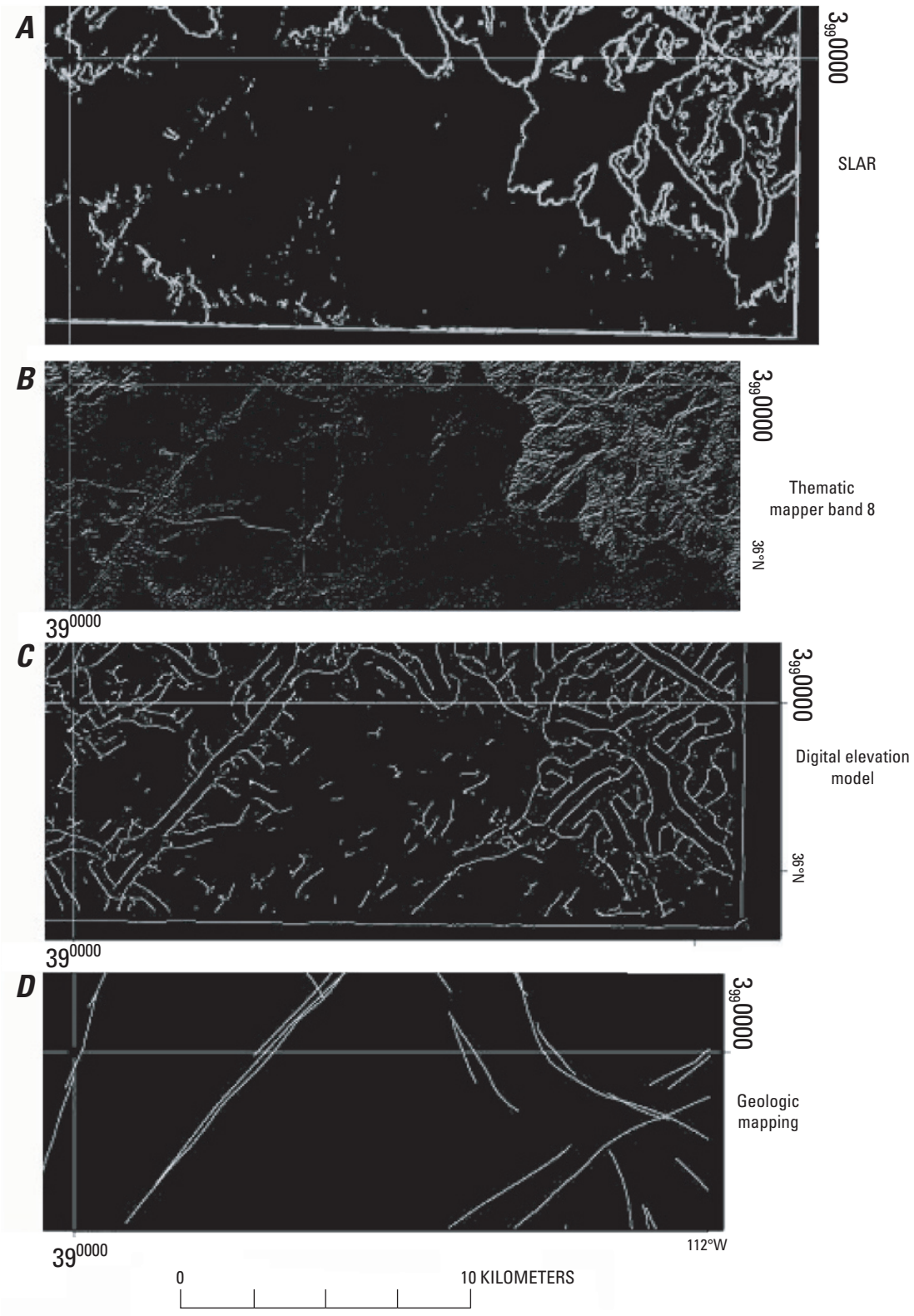


**Figure 7.** Lineaments obtained from mapping data for side-looking airborne radar (*A*), thematic mapper band 8 (*B*), digital elevation model (*C*), and geologic mapping (*D*). Images cover approximately the same area and are aligned by easting (meridians of longitude).

### Lineament Map

The lineament map is a line drawing on which all lineament-correlation data are summarized by mapping the computer-generated correlations by hand. In the focus area (fig. 1), this map, which is a scanned version of the original map, is named "fa_lin".

### Lineament-Overlay Map

The lineament-overlay map is a binary version of the lineament map designed to be overlaid on the other maps. The lineaments are assigned a value of 1, and everything else a value of 0. In the focus area (fig. 1), this map is named "fa_lin_overlay".

### Lineament Digital-Raster-Graphics Map

The lineament DRG map is the lineament-overlay map overlain on the DRG map. In the focus area (fig. 1), this map is named "fa_drg_lin".

### Lineament Normalized-Density-of-Vegetation-Index Map

The lineament NDVI map is the lineament map overlain on the NDVI map. In the focus area (fig. 1), this map is named "fa_ndvi_lin".

## Discussion

The images showing the derived deep- and shallow-data correlations superimposed on the (NDVI) maps show clearly that some correlations, where they intersect drainages, coincide with changes in the NDVI, so that the brightness (vegetation content) changes abruptly at the intersection of the drainage and the lineament (fig. 8). We interpret these points to occur where the lineament coincides with dams or springs in drainages, so that surface water is sufficiently close to the surface to support vegetation. The opposite situation also occurs, where the amount of vegetation decreases abruptly downstream of the lineament intersection. Surprisingly, many of the correlations that coincide with changes in NDVI have approximately east-westward trends because the east-west lineaments were believed to be a fabric in the basement and are not obvious on the surface without the methods used in this study. The NDVI maps also are a convenient means of locating some springs and seeps in the walls of the Grand Canyon.

The numerous of correlations in addition to those defined by surface geologic mapping lead us to ask whether these correlations are real or fortuitous. A contact in the basement between two contrasting rock types should not necessarily lead to offset and penetrative fracturing. We conclude, however, that most of the correlations are probably real for the following reasons. First, the geologic history, as discussed briefly above, documents numerous episodes of uplift, erosion (presumably differential, depending on rock type and degree of fracturing), subsidence, sedimentation, lithification, compression, and extension. With such a long history of repeated tectonic stress, we presume that virtually every fracture, zone of weakness, and even many contacts (surfaces of differing rock strengths) have probably moved in response. Second, our correlation maps correlate closely with the known tectonic features of fault zones and monoclines or are parallel to or strike extensions of known features. Late in this study, we discovered that the geologic map by Richard and others (2000) contained a substantial number of previously unmapped faults not shown on the maps we used in our analysis. Within the focus area (fig. 1), about 50 new faults (depending on how segments following the same strike are counted) are shown on Richard and others' map: and of these 50 faults, only three short segments were not detected at least in part by our correlations. Moreover, this study shows that many of the newly mapped faults have extensions not mapped on the surface and, in some places, nearby parallel structures.

If the correlations or a subset of them are fortuitous, then in such a large study area (fig. 1) they should show a near-random distribution because any correlations would not be connected by penetrative fractures. Correlations would occur where the (numerous) surficial fractures happened to overlie basement-rock physical-property contrast. To test whether the distribution of correlations was random, we used quadrat analysis, which we applied to the Grand Canyon 1º by 2º quadrangle to study the spatial distribution of all correlations generated between the geophysical-anomaly data and the surface-lineament data. We chose Grand Canyon quadrangle because it had the most numerous and visually the most random distribution of correlations. Quadrat analysis was applied to a 174- by 108-km area of the quadrangle; only a small area along the borders was omitted to use quadrats that contained exactly 100 rows and 100 columns in the 30-m-pixel-size correlation image—that is, 3- by 3-km quadrats—producing 2,088 quadrats. The minimum number of correlations in a quadrat was 11, and the maximum number was 4,420. The variance/mean ratio (Thomas and Huggett, 1980) of all correlations in the 2,088 quadrats is 523.3, indicating that the correlations follow neither a uniform (variance/mean ratio of 0) nor a random (variance/mean ratio of 1) spatial distribution in the quadrangle. Such a large ratio indicates that the correlations are nonrandom and strongly clustered spatially (Thomas and Huggett, 1980).

The methods used in this study to find candidate deep penetrative fractures are objectively obtained and repeatable, assuming that the same criteria are used for the definition of lineaments—that is, the same parameters. These methods do not, however, provide any information as to whether a given fracture is open or closed. In some places, time-domain elec-

trical sounding can detect whether or not a particular fracture is water filled; however, at present, no cost-effective method exists to survey such large areas as the study area (fig. 1). Furthermore, if a structure in the basement does not juxtapose rocks with differing density or magnetization, no geophysical anomaly will be detected, and so no deep lineament will correlate with surface lineaments. Thus, in combination with the lack of detailed spatial data coverage, probably many more candidate deep penetrative fractures are present than were mapped by this study. However, because of the large areal extent sampled and the multiple datasets utilized, we believe that all important deep-fracture-trend directions were likely to be detected by this study.

The density of correlations constitutes a crude estimate of "rechargeability," easily seen as contrasting areas of sparse or dense line occurrence in the line drawing of the focus area (fig. 9; see data archive for full-resolution version). "Rechargeability" estimates could be quantified by passing a window over the correlation grids and calculating the number of nonzero pixels within the window.

Close examination of figure 9 shows several types of correlation: (1) correlations of deep lineaments with surficial faults, folds, or lineaments that result in a line; and (2) correlations of deep lineaments with surficial joint patterns that result in echelon patterns or paths of jointlike correlation because of "smearing" of the deep-lineament location to account for the low-pass-filter effect of the gridding of geophysical data and the possible dip of structures. As discussed above in the section entitled "Methods," joints are generally believed to be penetrative as well as faults, so that correlations with surficial joints are as important as correlations with faults in terms of locating penetrative fractures. Study of the line drawing shows that existing joint systems have commonly accommodated faulting; in many places, a fault extension is due to correlation with joints. Several examples of a structure extending across the entire map as a combination of fault and joint correlations

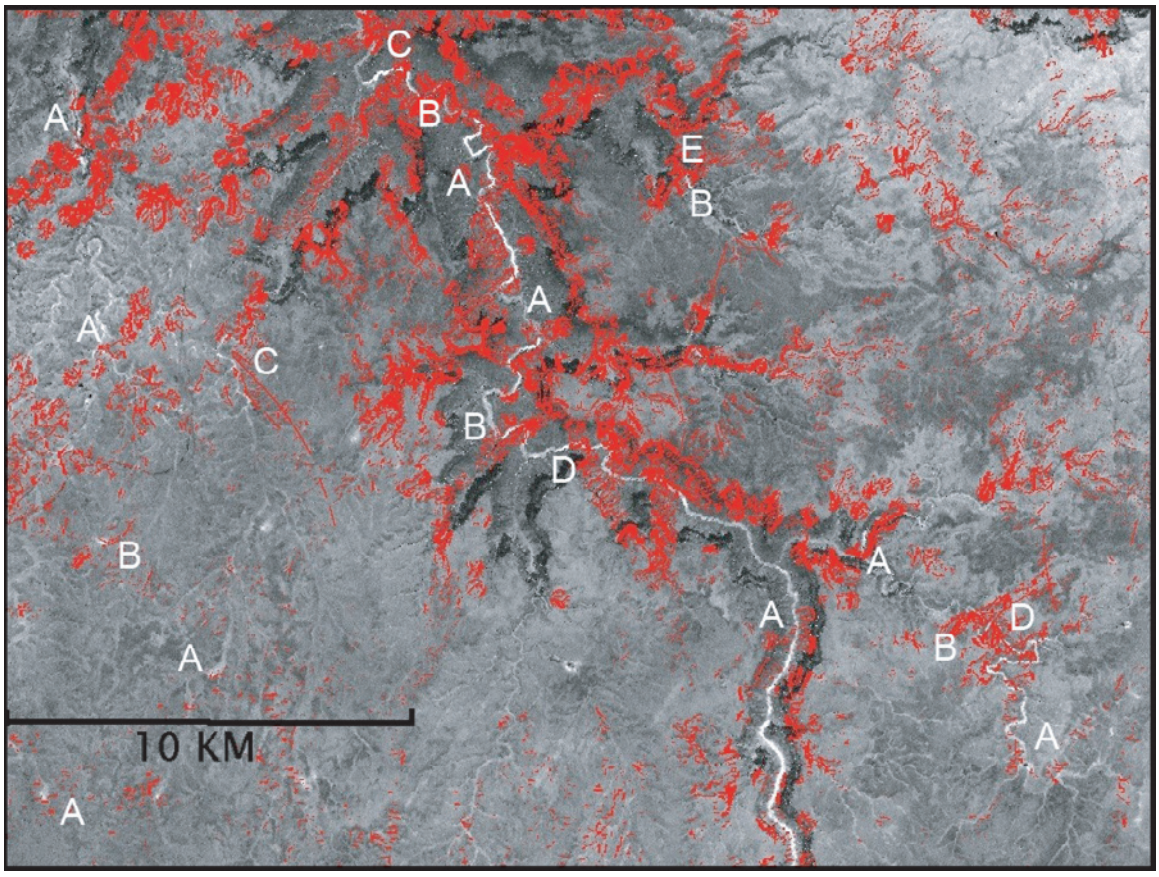


**Figure 8.** Normalized-density-of-vegetation-index (NDVI) image of Havasu Creek area just south of its confluence with the Colorado River in Grand Canyon National Park, Ariz. Red overlay is deep-geophysical/shallow-surficial-lineament-correlation dataset. Letters mark a sample of points where a nearby intersection of a red trend with drainage changes NDVI value in drainage, indicating a change in amount of vegetation and, by implication, of available near-surface water. Approximate trend directions: A, east-west; B, northeast-southwest; C, northwest-southeast; D, north-south; E, combination.

are visible in the line drawing. Examples of both types of correlation are shown in figure 10, together with "railroad-track correlations". These patterns occur because of discrepancies in the locations of fold axes and fault traces between the various geologic-map datasets due to differences in the scale and accuracy of compilation, and because of shallow dip in the basement structures. For areas outside the focus area (fig. 1), the various correlation maps can be used instead of the line drawing, which is, in fact, a highly simplified version of a correlation map, and so a full correlation map should be used instead, permitting the application of correlation rules, such as correlations from several datasets being more heavily weighted than only one correlation. Figure 9 does, however, have one advantage: it highlights some penetrative fractures that are traceable across the entire study area (fig. 1), in some places as fault/fold axes and elsewhere utilizing joints for some segment of the lineament. Several such features are visible in the NDVI map of the Havasu Creek area (fig. 8), especially with east-northeastward and north-southward directions.

All correlations were equally weighted in this study. However, we could have easily applied various weighting schemes to emphasize, for example, areas where more than one surficial dataset was correlated at depth, or where more than one deep dataset was correlated with shallow lineaments. Finally, using possibility theory (Kandel, 1982), we could make logical combinations of all the correlations at each pixel location to find both the best and poorest correlations according to some selected set of criteria or weighting rules. Such analyses can easily be carried out by using the "ARC grid" grids that give pixel-by-pixel correlations for the aeromagnetic, Bouguer gravity, and isostatic-gravity anomalies.

## Web-Site Design

The results of this work are archived here in the form of a Web site, constructed according to USGS standards and designed to be mainly accessed with a Web browser, either over a network or from a locally loaded DVD. Most of the Web site development was carried out by Christopher Call, whose notes and descriptions are attached in appendix 1.

## Conclusions

This study provides a method that yields a mathematical-lower-bound (not the least lower bound) set of candidate deep penetrative fractures except for coincidental correlations. All correlations are presented in datasets that can be used as layers in a GIS to assist in land-use planning. The locations of candidate deep penetrative fractures are shown at a resolution (pixel size) of 30 m but are subject to errors of as much as ±250 m due to the 500-m grid interval of the geophysical data defining deep structural boundaries.

Numerous new zones of possible deep fracturing in the study area (fig. 1) have been defined and are archived here in

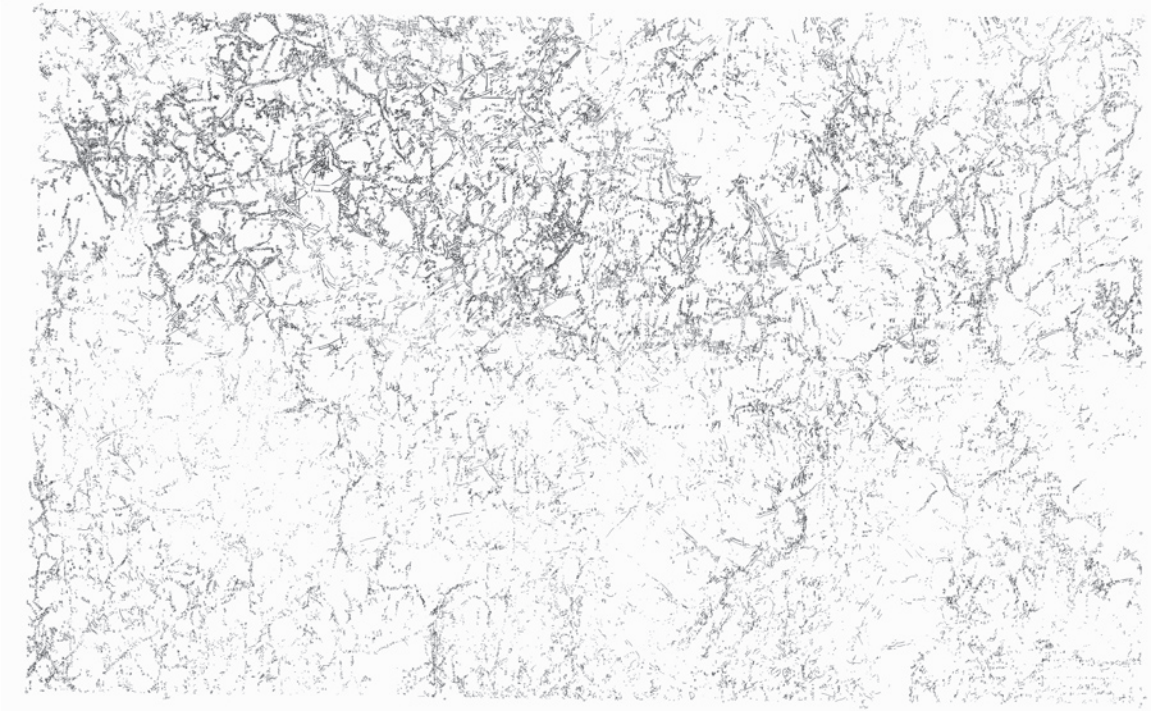

**Figure 9.** Line drawing showing correlations between deep- and shallow-lineament datasets for focus area (fig. 1), defining candidate deep fractures. Spatial density of correlations may estimate possibility of deep recharge. (See "Report Downloads" section of data archive.)

ARC/INFO grids that uniquely define which deep and shallow datasets correlate. The results are objectively obtained and repeatable as long as the same parameters are used. If other parameter sets are preferred, a different result with either more or fewer correlations would be obtained; nonetheless, the resulting correlations are objectively obtained and repeatable. We believe that the distribution of trends and the density of correlations would not change greatly for reasonable variations in the parameters used to set the threshold values for lineament definition.

The inferred lineaments appear to also control some near-surface water movement in many places. The spatial density of correlations gives a starting approximation of possible areas of poor and good recharge due to deep-fracture density. However, the data and analytical techniques used cannot predict whether the fractures are open or closed.

Future studies could calculate correlation-density maps for each of the sheets as an indication of recharge potential. Moreover, possibility theory from fuzzy logic, or some other schema of criteria, could be used to further quantify and discriminate the correlations. The data archived in this study should facilitate future research on the study area (fig. 1), such as optimal depth-to-basement calculations for the six quadrangles studied, and additional analysis of the data with regard to deep recharge of aquifers. Results from various phases of this study were presented by Gettings (2001, 2003a, b) and M.W. Bultman (written commun., 2003).

## References Cited


Arizona Geologic Survey and Bureau of Land Management, 1993, Arizona geologic map: Arizona Geological Survey Map 26, scale 1:100,000.

Babcock, R.S., 1990, Precambrian crystalline core, *in* Beus, S.S., and Morales, Michael, eds., Grand Canyon geology: New York, Oxford University Press, p. 11–28.

Beus, S.S., and Morales, Michael, eds., 1990, Grand Canyon geology: New York, Oxford University Press, 518 p.

Billingsley, G.H., 2000, Geologic map of the Grand Canyon 30′ × 60′ quadrangle, Coconino and Mohave Counties, northwestern Arizona: U.S. Geological Survey Geologic Investigations Series Map I–2688, 15 p., scale 1:100,000.

Blakely, R.J., 1995, Potential theory in gravity and magnetic applications: Cambridge, U.K., Cambridge University Press, 441 p.

Blakely, R.J., and Simpson, R.W., 1986, Approximating edges of source bodies from magnetic or gravity anomalies: Geophysics, v. 51, no. 7, p. 1494–1498.

de Marsily, Ghislain, 1986, Quantitative hydrogeology; groundwater hydrology for engineers (translated by Gunilla de Marsily): Orlando, Fla., Academic Press, 440 p.

European Space Agency, 2004, Spaceborne radar imagery: URL http://earth.esa.int/applications/data_util/SARDOCS/spaceborne/ [accessed 10/31/2004].

Gettings, M.E., 2001, An objective method of delineating trends in potential field data [abs.]: International Association of Geomagnetism and Aeronomy Joint Assembly, Hanoi, 2001, Abstracts, p. 251.

Gettings, M.E., 2003a, A method of delineating deep penetrative fractures in thick sedimentary rock sequences: International Union of Geodesy and Geophysics General Assembly, 23d, Sapporo, Japan, 2003, Scientific Program and Abstracts, p. B259.

Gettings, M.E., 2003b, Identification of possible deep penetrative fractures on the southwestern Colorado Plateau, U.S.A.: International Union of Geodesy and Geophysics General Assembly, 23d, Sapporo, Japan, 2003, Scientific Program and Abstracts, p. B257.

Grauch, V.J.S., and Cordell, Lindrith, 1987, Limitations of determining density or magnetic boundaries from the horizontal gradient of gravity or pseudogravity data: Geophysics, v. 52, no. 1, p. 118–121.

Hancock, P.L., 1969, Jointing in the Jurassic limestones of the Cotswold Hills: Geologists' Association of London Proceedings, v. 80, no. 2, p. 219–241.

Hirschberg, D.M., and Pitts, G.S., 2000, Digital geologic map of Arizona; a digital database derived from the 1983 printing of the Wilson, Moore, and Cooper 1:500,000-scale map: U.S. Geological Survey Open-File Report 00–409, 67 p.

Huntoon, P.W., 1990, Phanerozoic structural geology of the Grand Canyon, *in* Beus, S.S., and Morales, Michael, eds., Grand Canyon geology: New York, Oxford University Press, p. 261–309.

Ingebritsen, S.E., and Sanford, W.E., 1998, Groundwater in geologic processes: Cambridge, U.K., Cambridge University Press, 341 p.

Jaeger, J.C., and Cook, N.G.W., 1976, Fundamentals of rock mechanics (2d ed.): London, Chapman and Hall, 585 p.

Kandel, Abraham, 1982, The algebra of inexactness, chap. 2 *of* Fuzzy techniques in pattern recognition: New York, John


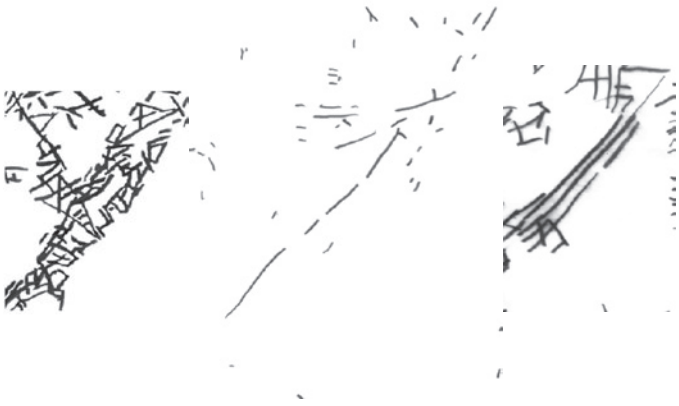

**Figure 10.** Examples of correlations from line drawing in figure 9. Left, correlation between deep lineaments and joint sets on surface; center, correlation with a surface fault, fold, or single fracture; right, multiple correlation ("railroad track") resulting from slight discrepancies in location of a fault in three different geologic databases.

Wiley & Sons, p. 22–90.
Kidwell, K.B., ed., 1990, Global Vegetation Index user's guide: Washington D.C., National Oceanic and Atmospheric Administration, National Climatic Data Center, Satellite Data Services Division, 45 p.
Lillesand, T.M., and Kiefer, R.W., 1994, Remote sensing and image interpretation (3d ed.): New York, John Wiley & Sons, 750 p.
Nabighian, M.N., 1972, The analytic signal of two-dimensional magnetic bodies with polygonal cross-section. Its properties and use for automated anomaly interpretation: Geophysics, v. 37, no. 3, p. 507–517.
Odling, N.E., Gillespie, P.A., Bourgine, Bernard, Castaing, Christian, Chiles, J.P., Christensen, N.P., Fillion, Eric, Genter, Albert, Olsen, Christian, Thrane, Lena, Trice, Robert, Aarseth, E.-S., Walsh, J.J., and Watterson, Juan, 1999, Variations in fracture system geometry and their implications for fluid flow in fractured hydrocarbon reservoirs: Petroleum Geoscience, v. 5, no. 4, p. 373–384.
Price, N.J., 1966, Fault and joint development in brittle and semi-brittle rock: Oxford, U.K., Pergamon Press, 176 p.
Price, N.J., 1974, The development of stress systems and fracture patterns in undeformed sediments, *in* Advances in rock mechanics: International Society for Rock Mechanics Congress, 3d, Denver, Colo., 1974, Proceedings, v. 1, pt. A, 487–496.
Richard, S.M., Reynolds, S.J., Spencer, J.E., and Pearthree, P.A., 2000, Geologic map of Arizona: Tucson, Arizona Geological Survey, scale 1:1,000,000.
Robson, S.G., and Banta, E.R., 1995, Ground-water atlas of the United States; segment 2, Arizona, Colorado, New Mexico, and Utah: U.S. Geological Survey Hydrologic Investigations Atlas HA–730–C, p. C1–C32 [URL http://capp.water.usgs.gov/gwa/index.html].
Sweeney, R.E., and Hill, P.L., 2001, Arizona aeromagnetic and gravity maps and data; Web site for distribution of data: U.S. Geological Survey Open-File Report 01–0081 [URL http://pubs.usgs.gov/of/2001/ofr-01-0081/.
Thomas, R.W., and Huggett, R.J., 1980, Modelling in geography; a mathematical approach: Totowa, N.J., Barnes and Noble Books, 338 p.

# Appendix 1. ArcGIS and Other Procedures Used for the Identification of Important Hydrologic Structures from Regional Geophysical Studies

By Christopher Call

Document-creation date: 2/4/03
Last modification: 6/25/03

This appendix contains the listed procedures for creating the shapefiles for the Identification of Important Hydrological Structures from Regional Geophysical Studies project.

## Procedure for creating the Study Area Boundary coverage (sapoly.shp) with geographic coordinates *(added 2/4/03, Chris Call)*

Took a coverage of the 1°×2° quadrangle sheets and selected the six (Grand Canyon, Marble Canyon, Holboork, Prescott, Williams, and Flagstaff) quadrangles and created a shape file from it by using ArcMap. The shapefile was then converted to an ArcInfo coverage and used as the polygon clip layer for the Study Area Reference Maps (geographic).

## Procedure for creating Study Area Reference Maps

Convert shapefiles to an ArcInfo coverage Polygon shapefiles that contain user-defined attribute data

**Arc: precision double double**
**Arc: shapearc azgeo.shp info_azgeo type**
**Arc: clean info_azgeo cl_azgeo # .0002 poly**
**Arc: regionpoly cl_azgeo final_azgeo type final_azgeo**

Point or Line shapefiles that contain user-defined attribute data

**Arc: precision double double**
**Arc: shapearc streams3.shp info_strm3**

Clipping of data

**Arc: clip final_azgeo studya sageo poly .0002** [for a polygon coverage]
**Arc: clip final_strm3 studya sastrm3 line .0002** [for a line coverage]
**Arc: clip final_town studya satown point .0002** [for a point coverage]

Converting the ArcInfo files back to shapefiles
Add the coverage to the ArcMap layer
Right-click on the table of contents on the layer
Select DATA then choose the EXPORT option

## Procedure for creating the utm500geo, utmfold, sa_500geo, sa_fold and sa_fault Study Area Reference Maps *(added 2/20/03, modified 2/28/03, Chris Call)*

## Procedure for creating az500geo and fold coverages

Imported the coverage files in ArcInfo
**Arc: import auto azgeol.e00 az500geo**
Converted the coordinate system [UTM zone 12; using ArcToolbox]
Performing the CLIP command in ArcInfo (for study-area coverages)
Used the projectdefine command in ArcInfo to assign a datum to the coverages
**Arc: defineprojection cover sa_utm500geo**
**Projection: datum nad27**
**Projection: parameters**
Used ArcToolbox to transform the projection to [UTM zone 12, NAD27 CONUS]
Built the coverages in ArcInfo
**Arc: build sa_500geo_utm poly**
The coverages were converted to shapefiles as described above

## Procedure for creating the polygon clip layer

Started with a copy of sapoly.shp and projected it to [North American Datum 1983.prj; using ArcToolbox]
Converted the coordinate system of sapoly.shp to [UTM zone 12; using ArcToolbox]
Converted the copy of sapoly.shp to an ArcInfo file (study_area) [ArcToolbox]

## Procedure for creating the sa_500geo and sa_fold coverages

Used same procedure for clipping data as described above
Used same procedure for converting ArcInfo coverages to shapefiles as described above

## Creation of the Fault coverages *(added 2/28/03, Chris Call)*

Selected all of the geologic boundaries that were faults
**Arc: reselect gcpoly gcfault line**
**>: res linetype cn 'NORMAL HIGH ANGLE FAULT' or linetype cn 'NORMAL HIGH ANGLE INFERRED FAULT' or linetype cn 'NORMAL HIGH ANGLE CONCEALED FAULT'**

**or linetype cn 'NORMAL REVERSE FAULT' or linetype cn 'NORMAL REVERSE INFERRED FAULT' or linetype cn 'NORMAL REVERSE CONCEALED FAULT' or linetype cn 'UNDERWATER FAULT'**
**>:**

Convert the coverage to a shapefile by using ArcToolbox

Source for az500geo and fold

A digital Database Derived from the 1983 printing of the Wilson, More, and Cooper 1:500,000-scale map (by D.M. Hirschberg and G.S. Pitts)

Downloaded from: http://geopubs.wr.usgs.gov/open-file/of00-409/

Source for gcgeo, gcfault, gcfold

Geologic Map of the Grand Canyon 30° × 60° Quadrangle, Coconino and Mohave Counties, Northwestern Arizona (by George H. Billingsley)

Downloaded from: http://pubs.usgs.gov/imap/i-2688/

## Exporting Oasis montaj maps as Shapefiles *(added 2/4/03)*

Display and select the map you want to export.

On the Map menu, click Export. The Export Map dialog box is displayed.

In the Output format box, select ArcView Shapefile (*.shp).

Click [OK]. In the Exported file name dialog box, specify the name (test.shp) to save the file as and a directory to save it in.

This creates (depending on the attributes included in the map) up to three different shape files and an index and database files as follows:

| | |
|---|---|
| test_ln.shp | lines |
| test_pg.shp | polygons |
| test_pt.shp | points |

## Procedure for producing Grids and Geotifs that contain either a fault or fold *(added 3/5/03, Chris Call)*

Select the desired 1° × 2° quadrangle from the Study Area shapefile (ArcMap, UTM coordinates)

Convert the selected quadrangle to a shapefile in ArcMap

Convert the quadrangle shapefile to a polygon coverage by using ArcToolbox

Clip the different faultline and foldline coverages by using the quadrangle coverage as the clip coverage in ArcInfo

Append all of the individual clipped coverages (from above step) into 1 coverage in ArcInfo (use the notest option)

**Arc: append hbrook notest**
**Enter the 1st coverage: hb_fault1**
**Enter the 2nd coverage: hb_fault2**
**Enter the 3rd coverage: hb_fold2**
**Enter the 4th coverage: end**

Build line topology for the created line coverage

**Arc: build hbrook line**

Add an attribute (FTFD) to the coverage's feature-attribute table

**Arc: additem hbrook.aat hbrook.aat**
**FTFD 3 3 I**

Assign a value of 255 to each tuple in the ftfd attribute (ArcMap)

Convert the line coverage to a grid using ArcToolbox

Let the "Value item:" be equal to FTFD
Cell size = 30
Background value = zero

Convert the grid to a TIFF image using ArcToolbox

Colormap = grayscale (256 color)
Image format = TIFF

## Procedure for importing data into ArcGIS from Oasis Montaj *(added 2/26/03, modified 3/4/03, Chris Call)*

Shaded reliefs

Export shaded relief from Oasis Montaj under the geotif format

Import into ArcMap

Shapefiles

Export point data from Oasis Montaj as an ArcView shapefile

Define projection [UTM zone 12, NAD27-CONUS] using ArcToolbox

Import into ArcMap

## Procedure for creating the geologic-contact-elevation coverage and then exporting it as an ASCII file *(added 3/19/03, modified 4/4/03, Chris Call)*

Start with the utm500geo coverages

Select all boundaries

**Arc: reselect utm500geo contact line**
>: res utm500geo# ge 0
**>:**

Copy the line and polygon FATs of utm500geo coverage

**Arc: Tables**
**Tables: copy utm500geo.pat geo.pat**
**Tables: copy utm500geo.aat geo.aat**

Eliminate the undesired columns from geo.pat

**Arc: dropitem geo.pat geo1.pat**
**Enter the 1st item: perimeter**
**Enter the 2nd item: utm500geo-id**

**Enter the 3rd item: source|**
**Enter the 4th item: area**
**Enter the 4th item:**
**Done entering item names (Y/N)? y**
**Do you wish to use the above items (Y/N)? y**

Copy geo.pat1 to Rgeo1 and Lgeo1 (one for the geology on the left and right)

Add 2 new columns to the FAT of Rgeo1 and Lgeo1 (Lpoly#, Rpoly#, Lunit, and Runit)

**Arc: additem Lgeo1.pat Lgeo2.pat Lpoly# 4 5 B**
**Arc: additem Lgeo1.pat Lgeo2.pat Lunit 10 10 C**
*Repeat the two additems except using Rgeo1.pat and Rgeo2.pat*

Copy the values of UTM500geo# to (Lpoly# and Rpoly#)

**Arc: Tables**
**Tables: select Lgeo2.pat**
**Tables: calc Lpoly = utm500geo#**

Copy the value of unit to Lunit and Runit

Eliminate the utm500geo# and unit columns from both Lgeo2.pat and Rgeo2.pat

Join the Lgeo2.pat and Rgeo2.pat tables to geo.aat

**Arc: joinitem geo.aat Lgeo2.pat L_geo.aat Lpoly#**
**Arc: joinitem L_geo.aat Rgeo2.pat line_geo.aat**

Add a new column **(contact#)** to ln_geo.pat

**Arc: additem line_geo.aat lngeo.aat contact# 4 5 B**

Copy the values of UTM500geo# to contact#

Drop the undesired columns from the lngeo.aat table

**Arc: dropitem lngeo.aat lngeo1.aat**
**Enter the 1st item: fnode#**
**Enter the 2nd item: tnode#**
**Enter the 3rd item: lpoly#**
**Enter the 4th item: rpoly#**
**Enter the 5th item: length**
**Enter the 6th item: utm500geo#**
**Enter the 7th item: utm500geo-id**
**Enter the 8th item: linecode**
**Enter the 9th item: source**
**Enter the 10th item:**
**Done entering item names (Y/N)? y**
**Do you wish to use the above items (Y/N)? y**

Join the lngeo1 table with the FAT of the contact coverage (contact.aat)

**Arc: joinitem contact.aat lngeo1.aat contact.aat contact#**

Convert the line coverage (contact) to a point coverage (contactpt)

**Arc: arcpoint contact contactpt line contact#**

Add a new column (ctpt#) to contactpt.pat

**Arc: additem contactpt.pat contactpt.pat ctpt# 6 6 I**

Copy the values from ct# to ctpt# (in tables) for contactpt.pat

Copy the FAT of contact to a temp file

**Arc: copyinfo contact.aat temp**

Add a new column (ctpt#) to the temp file

**Arc: additem temp temp ctpt# 6 6 I**

Copy the values from ct# to ctpt# (in tables) for temp

Remove the unwanted columns from the temp file (save only Lunit, Runit, and ctpt#)

Join the temp file to contactpt.pat using ctpt#

**Arc: joinitem contactpt.pat temp contactpt.pat ctpt#**

Convert the contactpt coverage to a grid (grd_contactpt) with a cell size of 25 m using ArcToolbox

Convert the AZDEM cell size to 25m

**Arc: grid**
**Grid: azdem25m = resample (azdem, 25)**

Create an ASCII file of the contact, using the "select" command. This file will have the unique identifier (for geology), x, y, and elevation columns.

**Arc: grid**
**Grid: geoel = select(grd_contactpt, azdem25m)**

Open geoel in Wordpad (or any other text-editing program)

In WordPad, click the 'Save As' command and save it as a Unicode Text

Document (This worked the first time I did this but not when I tried it a second time. If it doesn't work, then try opening it in Excel or Access and save it as comma-delimited text (csv)

Open ArcMap and add the text document (geoel)

Right click on the text document (geoel) and select 'Display X Y data' (to add the point data)

Convert the displayed points to a shapefile (geoel, in ArcMap)

Convert the shapefile to a point coverage by using ArcToolbox (azgeoel)

Define projection by using ArcToolbox (UTM, Zone 12, NAD27 – CONUS)

Create columns, elevation, and contactpt#

**Arc: additem azgeoel.pat azgeoel.pat contact pt# 4 5 B**
**Arc: additem azgeoel.pat azgeoel.pat elevation 12 12 C**

Copy values from azdem25m to elevation (in Tables)

Copy values from contactpt_ to contactpt# (in Tables; Contactpt_ is the column that contains the geology information.)

Delete the contactpt_ and azdem25m columns from the azgeoel.pat table

*If working with a smaller subset, skip to extra steps below, then continue here*

Copy the contactpt table to georelate.pat (in Tables)

Delete the area, perimeter, contactpt-id, the contact# columns (all unnecessary) from georelate.pat

Join azgeoel.pat to georelate.pat

**Arc: joinitem azgeoel.pat georelate.pat azgeoel.pat contactpt#**

(This process can take a long time.)

Copy azgeoel.pat to geology_elevation (in Tables)

Delete (dropitem) all of the columns except for x, y,

Lunit, Runit, and Elevation (in Arc)

Create four columns (utm_x, utm_y, long, lat)

**Arc: additem azgeoel.pat azgeoel.pat utm_x 12 12 N 3** (repeat for utm_y)

**Arc: additem azgeoel.pat azgeoel.pat long 11 11 N 5** (repeat for lat)

Change the projection of azgeoel to geographic (datum = NAD27, in ArcToolbox)

Add XY coordinates to geographic_azgeoel (in ArcToolbox)

Copy the values: x = utm_x, y = utm_y, x-coord = long, and y-coord = lat (in Tables or ArcMap)

Remove the columns: x-, y-, x-coord, and y-coord (in Arc or ArcMap)

Copy the FAT of geographic_azgeoel to geog_azgeoel (in Arc)

**Arc: copyinfo geographic_azgeoel.pat geog_azgeoel**

Delete all the columns except for elevation, Lunit, Runit, utm_x, utm_y, long and lat (in Tables or ArcMap)

Convert azgeoel to a shapefile (using ArcToolbox or ArcMap)

Open geogr_azgeoel table in ArcMap (if not already opened)

When viewing the attribute table (in ArcMap), click on the options button and select export. Export the data as a text file. (I prefer this way because the column headers are included in the ASCII file)

A second way to export data as an ASCII file (azgeoel_ascii)

**Arc: tables**
**Tables: select azgeoel_ascii**
**Tables: unload azgeoel_ascii_table**

If working with a smaller area, follow these steps, then proceed where you left off:

Clip the desired portion of data

**Arc: clip azgeoel grca_studyarea gc_azgeoel .00002**

**Arc: clip contactpt grca_ studyarea gc_contactpt .00002**

Continue to follow the other steps but use these file names instead of the ones listed

## Procedure for creating road coverages from TIGER census data *(added 4/11/03, last modified 4/22/03)*

Download the data from the census Web site and unzip the data

*http://www.census.gov/geo/www/tiger/tiger2k/othertgr.html*

Convert the TIGER data to a coverage and select the "join all tables" option (ArcToolbox)

Make a coverage of the line data included in the polygon coverage

**Arc: reselect Navajo_poly Navajo_line line**
**>: res Navajo_poly# ge 1**
**>:**

Start ArcMap and open the Navajo_line coverage

Select all of the records that have a value of A## *[## can be any two- digit number]* in the CFCC column (ArcMap, select by attribute CFCC <= A74; all roads have an 'A' as the first character in the CFCC column)

Create a new shapefile from the selected features (ArcMap, right click on Navajo_line and click on the export option, give it a name, and add it to the data frame)

Open the attribute table, and scroll through the table, and select all of the records that have names 'United States Highway #', 'State Highway #', 'County Road #', 'I-#', 'State Route #' or 'Route #')

Create a new shapefile from the selected features and delete roads that are not important, in an edit session (ArcMap).

Oftentimes it will be necessary to fill in missing gaps. To do this, start an editing session and screen-digitize the remaining segments of the road, or you can select the necessary segments to make the highway complete in an edit session (ArcMap)

Repeat for every county

After completing a road shapefile for every county, append all of the counties together (ArcToolbox or ArcInfo).

First, convert all of the shapefiles into coverages

Second, delete the columns "*shapefile_name_*" and "*shapefile_name*_id"; these are the only two fields in the coverage that are different from the others. For example, if your shapefile is named "Navajo_line", then you will need to delete the columns 'navajo_line_' and 'Navajo_line_id'.

Third, append all of the coverages together

**Arc: append append_road line none**
**Enter the 1st coverage: Navajo_rd**
**Enter the 2nd coverage**: *{Enter the remaining coverages and type'* **End***' after the last coverage}*

Define the projection of the appended coverage (append_road) to Geographic, NAD83 (ArcToolbox)

Change the projection of append_road to UTM zone 12 NAD83 (ArcToolbox)

Clean the append_road coverage. (It is important to be careful when using the "clean" command. I set the fuzzy tolerance and dangle length to 15 m, much smaller than the default setting for this coverage. "Clean" will not work properly if it has a geographic coordinate system; use ArcInfo or ArcToolbox instead.)

**Arc: clean append_road clean_rd 15 15 line**

Change the projection back to geographic and convert to a shapefile (ArcToolbox)

## Procedure for making the Lineaments map, in Photoshop *(added 6/25/03, last modified 6/25/03)*

Take the mylar copy of the map and scan it (It should be scanned as a grayscale; I used the scanner on the 1st floor of the USGS building in Tucson, AZ)

Save the map as a TIFF file and import it into Photoshop (Note: I could not open the scanned TIFF file directly into Photoshop for some strange reason and, so I imported it into Adobe Illustrator and saved it in Illustrator format and then imported that file into Photoshop.)

Once the file is imported into Photoshop, save it in Photoshop (.PSD) format

Create a new white background layer

Use the Eraser tool to erase dark areas between the lines. Leave all light to medium-gray areas but erase all nonlines that are black-gray to black and (or) areas that are darker than the lines. Erase all spaces between lines that are from 3 to 5 pixels long, and do this for the entire map. I used a 200% zoom.

Flatten the layers together (**Layer**, *flatten image*)

After preparing the map, the above step, select areas that have similar line thickness, Backgrounds, and line shades

Once selected, adjust the brightness/contrast and the gradient map for the image. Adjust *brightness/contrast* and the *gradient map* by clicking on the **Image** menu and click on the *adjust* option and then click on the function that you would like to use. In lighter regions, I would start by decreasing the brightness to between –25 and –35 (darkens the image) and then changing the gradient map (white ~15–35 and black ~95–90). When adjusting the gradient map click on the default gradient map (don't use the default) to get all of the options, see the images below. Change the gradient map to black and white; then you can adjust the levels (the bottom slides). I would then repeat the process, with making the image darker and then changing the gradient map, except that I would set the gradient map values to white ~40–60 and black ~60–40 (that is, I would make it into a black-and-white image). Sometimes I would have to do it three times, adding an inbetween step with gradient values of white ~30–45 and black ~90–70. For the dark areas I would follow the same process, but instead of making the image darker, I would make it lighter. This is the general guideline, but each section was unique and required individual tweaking. In general, the smoothness of the image increases with the more times the gradient map is performed. After completing each section, inspect the changes by looking at the image before any editing and after editing. There will probably be a few places that will require touchup with either the eraser or paintbrush (for example, a too-thin line).

After adjusting the brightness/contrast and the gradient map for the entire image (in separate pieces), select the entire image and adjust the gradient map to black = 50 and white =50.

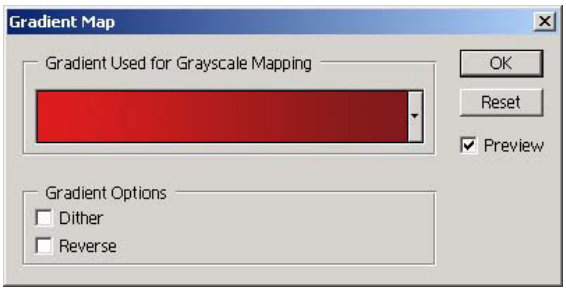


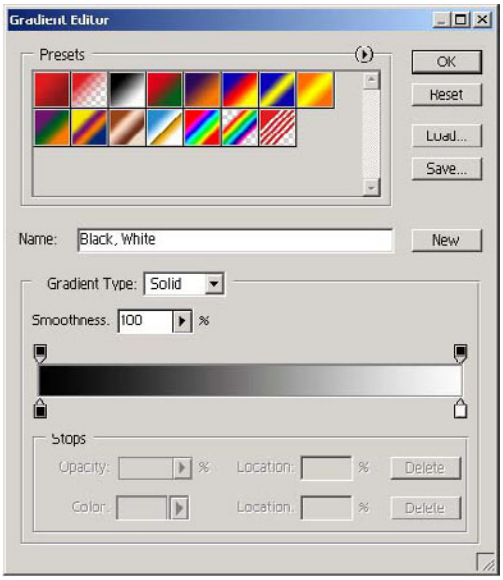


Click on the Red map to get the screen to the right. This is the gradient-map-editor screen

## Georeferencing an Image, specifically the Four Corners geologic map *(added 6/26/03)*

Before starting, find tickmarks with known coordinates

Start ArcInfo

**Arc: register cornergeo.tif # # composite # # #**

The Register Windows appear.

Follow the directions given in the help documents (Look up 'register')